J Appl Electrochem (2010) 40:59–63
DOI 10.1007/s10800-009-9967-2

ORIGINAL PAPER

Hydrothermal preparation of Zn_2SnO_4 nanocrystals and photocatalytic degradation of a leather dye

Edson Luiz Foletto · Sérgio Luiz Jahn · Regina de Fátima Peralta Muniz Moreira

Received: 16 July 2008 / Accepted: 7 July 2009 / Published online: 18 July 2009

Abstract Zinc stannate (Zn_2SnO_4) powder was prepared by a hydrothermal process at 200 °C for 12 h. The material was characterized by X-ray-diffraction (XRD) and N_2 adsorption–desorption isotherms. The synthesized sample presented a pure phase, an average nanocrystal size of about 19 nm, a surface area (BET) of about 41.8 $m^2\ g^{-1}$ and total pore volume of about 0.19 $cm^3\ g^{-1}$. Its photocatalytic activity was tested by the degradation of the leather azo-dye, Direct Black 38, in aqueous solution under UV irradiation. Adsorption kinetic data showed that the pseudo-second-order model was the most appropriate for the dye studied. Adsorption onto the Zn_2SnO_4 surface followed the Langmuir isotherm. The catalyst showed highly photocatalytic activity towards degradation of the dye, almost equal to that of the TiO_2-P25 Degussa photocatalyst. The results indicate that Zn_2SnO_4 could be employed for the removal of dyes from wastewaters.

Keywords Zn_2SnO_4 · Synthesis · Photocatalysis · Degradation · Dye

1 Introduction

Dye effluents may present certain environmental problems. For example, the presence of color may reduce aquatic diversity by blocking the passage of light through the water. Conventionally, dye wastewaters discharged by the textile and leather industry are treated using various chemical and physical methods, such as chemical coagulation, biological treatment, adsorption, ultrafiltration [1–5]. However, these processes have only limited success.

In recent years, attention has been focused on heterogeneous photocatalysis for the treatment of dye wastewaters. Several studies on photocatalytic degradation of dyes using semiconductor materials have been reported [6–9]. Semiconductor oxides and sulfides such as ZnO, Fe_2O_3, ZnS, CdS have been used, but among the photocatalysts, TiO_2 is one of the most used due to its high photocatalytic activity. Doping or combining TiO_2 with various metal ions such as Pt, Au, Co, Cu has been reported to be beneficial [10–14].

As an important member of transparent semiconductor materials, Zn_2SnO_4 is known to have high electrical conductivity, high electron mobility and low visible absorption [15–17], which makes it suitable for a wide range of applications, such as gas-sensing material [18], as anode material for Li-ion batteries [19] and as a photocatalyst for degradation of benzene in an aqueous solution [20]. It is usually prepared by solid-state calcination between ZnO and SnO_2, at high temperatures (higher than 1,000 °C) [21]. However, this conventional method presents disadvantages such as difficulty in obtaining a pure phase and the need for very high reaction temperatures [22].

In this study Zn_2SnO_4 was synthesized by the hydrothermal method at 200 °C for 12 h. The characterization of this material and its photocatalytic activity in the degradation of azo leather dye, Direct Black 38, was investigated.

E. L. Foletto (✉) · S. L. Jahn
Department of Chemical Engineering, Federal University of Santa Maria, Santa Maria, RS 97105-900, Brazil
e-mail: foletto@smail.ufsm.br; efoletto@hotmail.com

R. de Fátima Peralta Muniz Moreira
Department of Chemical and Food Engineering, Federal University of Santa Catarina, Florianópolis, SC 88040-900, Brazil

2 Experimental

2.1 Catalyst preparation

The nanosized Zn_2SnO_4 photocatalyst was prepared using the hydrothermal method. Zinc acetate ($ZnAc_2{\cdot}2H_2O$, analytical grade) and tin tetrachloride ($SnCl_4{\cdot}5H_2O$, analytical grade) were used as zinc and tin sources, respectively without further purification. The reaction system composition used to synthesize the Zn_2SnO_4 catalyst was as follows:

$1SnO_2{:}2.33ZnO{:}360H_2O{:}8.3NaOH$

The amount of reagents used was calculated based on the reaction stoichiometry (Eq. 1).

$$2ZnAc_2 + 1SnCl_4 + 8NaOH \rightarrow Zn_2SnO_4 + 4NaAc + 4NaCl + 4H_2O \quad (1)$$

The zinc acetate aqueous solution was added into tin tetrachloride aqueous solution slowly. Sodium hydroxide (NaOH) solution used as mineralizer was added dropwise into the mixture under magnetic stirring, resulting in a pH of 7.5. The final mixture was charged into a PTFE-lined stainless autoclave and the hydrothermal reaction was carried out at 200 °C for 12 h. Subsequently, the autoclave was allowed to cool naturally. The precipitate was filtered, washed with distilled water, and dried at 120 °C for 10 h.

2.2 Characterization methods

Nanopowder was characterized by X-ray diffractometry (XRD) (equipment Shimadzu model XD-7, with Cu Kα radiation). The average size of the Zn_2SnO_4 spinel crystallite was determined through the Scherrer equation: $D = K\lambda/(h_{1/2}\cos\theta)$, where D is the average crystallite size, K the Scherrer constant (0.9), λ the wavelength of incident X-rays (0.15405 nm), $h_{1/2}$ the peak width at half height and θ corresponds to the peak position (in this work, $2\theta = 34.29$).

N_2 adsorption–desorption isotherm measurements were carried out at 77 K using an Autosorb (Quantachrome) apparatus.

2.3 Materials and photoreactor

Direct Black 38, an azo dye extensively used in the leather industry, was used as the model compound. The chemical structure of the dye is given in Fig. 1. The photocatalytic activity of the commercial TiO_2 Degussa P25 was also evaluated and compared with that of Zn_2SnO_4. TiO_2 Degussa P25 is mostly in the anatase form (80% anatase form and 20% rutile) and has a BET surface area of 50 $m^2\ g^{-1}$ corresponding to a mean particle size of ca. 30 nm, and mean pore diameter of about 6.9 nm. The reactor was a commercial photochemical reactor (Hereaus UV-RS-1) of 500 mL, irradiated by a 150 W high-pressure mercury vapor lamp and light intensity was 4.04×10^{-4} Einstein min^{-1} [23]. The UV lamp was surrounded by a quartz thimble in the center of the reactor to ensure a homogeneous radiation field inside the reactor. A cylindrical jacket located around the plugging tube contained circulating water to absorb radiation and avoid heating of the solution. The temperature of the reaction medium was maintained at 298 K. The volume of the aqueous solution of dye was 400 mL to which 0.4 g of catalyst was added. The solution was magnetically stirred.

2.4 Adsorption tests

For the adsorption tests, 0.4 g of catalyst was added to 400 mL of the aqueous solution of dye at different initial concentrations and at pH 2.5, which was adjusted by using dilute H_2SO_4. The resulting solution was then stirred continuously at constant temperature (25 ± 2 °C) in the dark to achieve the adsorption equilibrium of dye on the catalyst. During the runs, 5 mL samples of solution were withdrawn at regular intervals and were centrifuged and filtered through a 0.22 μm PVDF membrane (Millipore) to completely remove catalyst particles. The amount of adsorbed dye on the catalyst surface was determined by mass balance. UV-vis absorption spectrum of Direct Black 38 aqueous solution at pH 2.5 was shown in a previous study [24]. The UV-vis absorption of dye is characterized by one band in the visible region, with its maximum located at 590 nm and by one band in the ultraviolet region

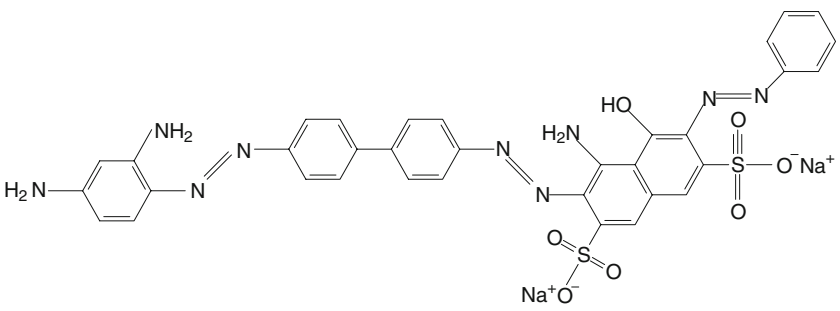

Fig. 1 Chemical structure of azo dye

with its maximum at 310 nm [25]. All samples were analyzed using a Shimadzu 1650C UV spectrophotometer at $\lambda_{max} = 590$ nm.

3 Results and discussion

3.1 Catalyst characterization

The XRD pattern for Zn_2SnO_4 is shown in Fig. 2. All the diffraction peaks can be perfectly indexed to cubic spinel-structured Zn_2SnO_4 (JCPDS Card No. 74-2184). The peaks and intensities of the produced powder and that of standard were the same. This indicates that there was a complete formation of the spinel phase in the obtained sample. The Zn_2SnO_4 lattice constant obtained by refinement of XRD data for the synthesized Zn_2SnO_4 was $a = 8.65$ Å (JCPDS Card No. 74-2184). The route of hydrothermal synthesis employed in this study presents the advantages of obtaining phase-pure Zn_2SnO_4, with the use of lower reaction temperatures. The crystal size was about 19 nm, as determined by the Scherrer equation.

Representation of nitrogen adsorption–desorption isotherms of Zn_2SnO_4 is shown in Fig. 3. The isotherms can be classified as type II, indicating a microporous structure. The BET area surface was found to be 41.8 $m^2\ g^{-1}$, and the total pore volume was 0.19 $cm^3\ g^{-1}$.

3.2 Removal by adsorption

Adsorption of dyes on the semiconductor surface is an important parameter in heterogeneous photocatalysis. Adsorption tests were carried out in order to evaluate the equilibrium constants. The influence of contact time on dye removal by Zn_2SnO_4 is presented in Fig. 4. It can be seen that the material was efficient in adsorbing dye and the process gradually attained equilibrium. The time profile of dye removal was a single, smooth and continuous curve leading to saturation. Figure 4 also shows that the contact time required to attain equilibrium was about 120 min for all the initial concentrations of dye.

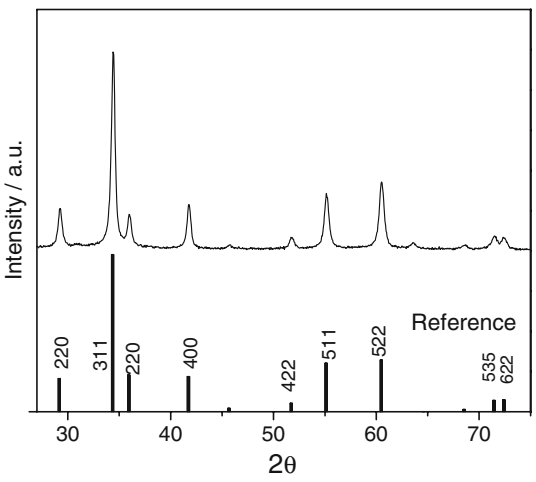

Fig. 2 Powder XRD pattern of Zn_2SnO_4 and reference Zn_2SnO_4 (JCPDS Card No. 74-2184)

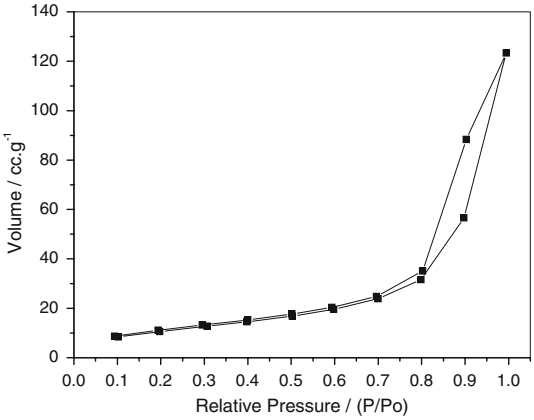

Fig. 3 Nitrogen adsorption–desorption isotherms for Zn_2SnO_4

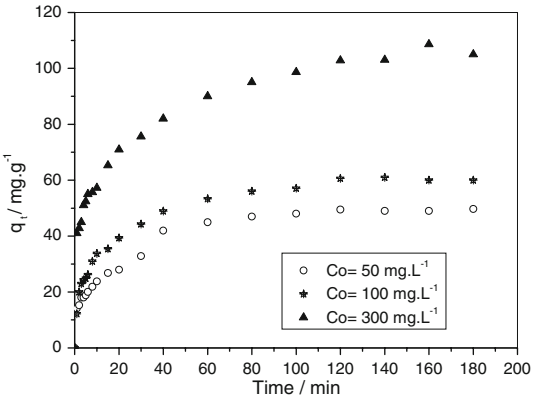

Fig. 4 Kinetic adsorption of Direct Black 38 on Zn_2SnO_4 with different initial dye concentrations ($Zn_2SnO_4 = 1$ g L^{-1}; pH 2.5; $T = 25$ °C)

Adsorption kinetic data were modelled using pseudo-first- and pseudo-second-order kinetic equations [26, 27]. Values of the rate constant (k_1), equilibrium adsorption capacity (q_e) and the correlation coefficient (r^2) were calculated from the plots of $\log(q_e - q_t)$ versus t (for the pseudo-first-order) and t/q_t versus t (for the pseudo-second-order) for each initial concentration of dye and are presented in Table 1. The calculated q_e values for the pseudo-first-order model do not agree with experimental values (Table 1). The plots of t/q_t versus t showed a linear relationship with correlation coefficients higher than 0.99 for the pseudo-second-order kinetic model. The calculated q_e values agree very well with the experimental data (Table 1)

Table 1 Adsorption kinetic parameters for each initial concentration of dye in solution

Concentration dye (mg L^{-1})	First-order kinetic model				Second-order kinetic model		
	q_e (exp.) (mg g^{-1})	k_1 (min^{-1})	q_e (calc) (mg g^{-1})	r^2	k_2 (g mg^{-1} min^{-1})	q_e (calc) (mg g^{-1})	r^2
50	49	0.028	33.95	0.971	2.35×10^{-3}	52.6	0.999
100	61	0.027	46.19	0.995	2.48×10^{-3}	62.5	0.999
300	103	0.029	73.42	0.992	1.53×10^{-3}	107.0	0.999

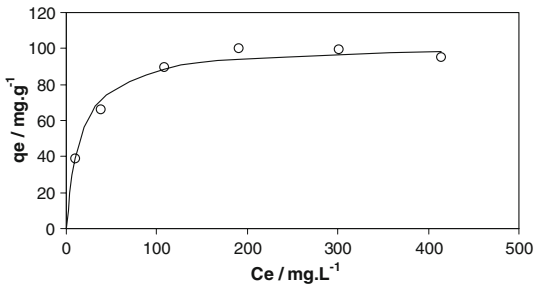

Fig. 5 Direct Black 38 adsorption isotherms on Zn_2SnO_4 (pH 2.5; $T = 25$ °C). *Open-circle* data points correspond to the experimental data and the line was plotted using the Langmuir model

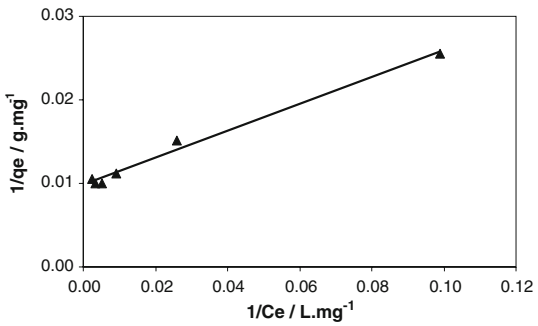

Fig. 6 Langmuir model

and this indicates that the adsorption of dye on Zn_2SnO_4 follows a pseudo-second-order model.

Figure 5 shows adsorption isotherms that express the adsorbed amounts as a function of the equilibrium concentration for Direct Black 38 in solution. Using the Giles classification [28], the isotherms obtained in the present work are the Langmuir type (L) with an initial concavity to the concentration axis. The L-shape isotherm means that there is no strong competition between the solvent and the dye to occupy the Zn_2SnO_4 surface sites.

The data obtained from the adsorption experiments were fitted to the Langmuir model (Eq. 2) [29]:

$$q_e = \frac{q_m b C_e}{1 + b C_e} \quad (2)$$

where C_e is the concentration of the dye in solution at equilibrium (mg L^{-1}), q_e is the amount of dye adsorbed per unit weight of the catalyst at equilibrium (mg g^{-1}), b is the Langmuir adsorption constant (L mg^{-1}), and q_m is the amount of dye adsorbed corresponding to monolayer coverage (mg g^{-1}).

The linear plot of $1/q_e$ versus $1/C_e$ (Fig. 6) shows that adsorption follows the Langmuir isotherm model. The fitting of experimental data to the Langmuir model resulted in maximum adsorption capacity (q_m) of 102 mg g^{-1} and $b = 0.061$ L mg^{-1}. In a previous study, Moreira et al. [24] found $q_m = 154$ mg g^{-1} for the adsorption of Direct Black 38 dye on Degussa P25 catalyst, under the same experimental conditions as used in this study.

3.3 Photodegradation study

The photocatalytic activity of Zn_2SnO_4 was evaluated by the degradation of Direct Black 38 azo-dye in aqueous solution, and was compared with that of commercially available Degussa-P25 catalyst. At the beginning of the experiments, 0.4 g of catalyst and 400 mL of the dye solution were fed into the photoreactor. The pH was adjusted to 2.5 by using dilute H_2SO_4. The dye solution was then magnetically stirred in the dark for 120 min before irradiating the photoreactor to make sure that the adsorption equilibrium was reached. Samples were periodically taken from the reactor, centrifuged and filtered through a 0.22 μm PVDF membrane (Millipore) before being subjected to a UV-vis spectrophotometer (Shimadzu 1650C UV, at $\lambda_{max} = 590$ nm. The initial dye concentration in the solution was 100 mg L^{-1}.

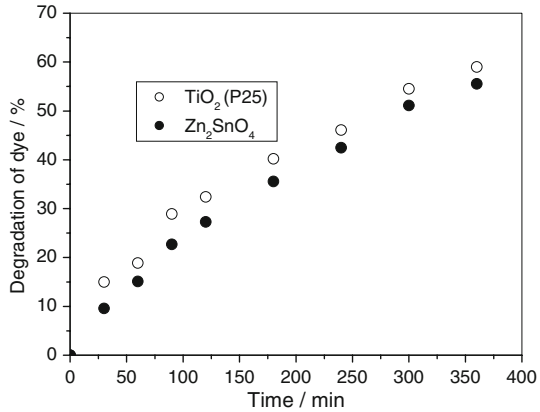

Fig. 7 Degradation rate of azo dye for the two catalysts

The photocatalytic degradation performance of the process was defined as % Degradation $= (A_0 - A)/A \times 100$, where A_0 is the initial absorbance and A is the final absorbance. The degradation of the dye molecules was negligible by direct photolysis. A degradation of the dye was only observed with the simultaneous presence of catalyst and UV-light.

The evolution of the dye degradation with irradiated time for both photocatalysts is shown in Fig. 7. The photocatalytic activity of Zn_2SnO_4 was almost equal that of the TiO_2-P25 photocatalyst, which may be attributed to its high specific surface area (41.8 $m^2\ g^{-1}$), high crystallinity and nanometric particle size (about 19 nm). The performance of a photocatalyst in the degradation of dyes is a complex function involving many parameters such as morphology of the particle surface, surface charge density, dye adsorption capacity of the material, which is related to the BET surface area, and pore size distribution. Lou et al. [30] observed that Zn_2SnO_4 nanocrystals exhibited high photocatalytic activity to various reactive dyes such as Reactive Turquoise Blue K-NR, Reactive Turquoise Blue B-RN, and Reactive Black B-GFF because of their great specific surface area (about 62 $m^2\ g^{-1}$). Zhang et al. [31] observed that oxide coupled ZnO–SnO_2 nanocrystals had equally excellent photocatalytic activity for the degradation of methyl orange when compared to TiO_2-P25.

4 Conclusions

Photocatalyst nano material was successfully prepared through a low temperature hydrothermal process. The synthesized material presented a pure phase and the mean nanocrystal size was of nanometric scale. An evaluation of adsorption and photocatalytic degradation of a direct dye using Zn_2SnO_4 as catalyst showed that a pseudo-second-order model best described the adsorption kinetic data. The equilibrium adsorption was described according to the Langmuir model and the monolayer coverage capacity was 102 mg of dye per gram of Zn_2SnO_4. The oxide produced showed efficient catalytic activity in degrading the azo-dye in aqueous solution, to an extent almost equal to that of commercially available TiO_2-P25 Degussa. Thus, nano Zn_2SnO_4 is a promising candidate for the photodegradation of dyes from wastewaters.

Acknowledgment The authors are grateful to the Brazilian research funding, CNPq, for financial support.

References

1. Lin SH, Lou CC (1996) Environ Technol 17:841
2. Demanin TR, Uhrich KD (1988) Am Dyest Report 77:13
3. Papic S, Koprivanac N, Bozic AL (2000) J Soc Dye Color 116:352
4. Mohorcic M, Teodorovic S, Friedrich VJ (2006) Chemosphere 63:1709
5. Bielska M, Prochaska K (2007) Dye Pigment 74:410
6. Hachem C, Bocquillion F, Zahraa O (2001) Dye Pigment 49:117
7. Sauer T, Neto GC, José HJ, Moreira RFPM (2002) J Photochem Photobiol A 149:147
8. Akyol A, Yatmaz HC, Bayramoglu M (2004) Appl Catal B 54:19
9. Chakrabarti S, Dutta BK (2004) J Hazard Mater 112:269
10. Sclafani A, Herrmann JM (2004) J Photochem Photobiol A 113:181
11. Subramanian V, Wolf EE, Kamat PV (2001) J Phys Chem B 105:11439
12. Caimei F, Peng X, Yanping S (2006) J Rare Earths 24:309
13. Colón G, Maicu M, Hidalgo MC (2006) Appl Catal B 67:41
14. Kryukova GL, Zenkovets GA, Shutilov AA, Wilde MW, Günther K, Fassler D (2007) Appl Catal B 71:169
15. Barth TFW, Posnjak E (1932) Z Kristallogr 82:325
16. Coffen WW (1953) J Am Ceram Soc 36:207
17. Poix P (1965) Ann Chim (Paris) 10:49
18. Yu JH, Choi GMJ (2002) J Electroceram 8:249
19. Belliard F, Connor PA, Irvine JTS (2000) Solid State Ionics 135:163
20. Wang C, Wang X, Fu J (2002) J Mater Sci 37:2989
21. Hashemi T, Al-Allak HM, Illingsworth J, Brinkman AW, Woods J (1990) J Mater Sci Lett 9:1776
22. Fang J, Huang A, Zhu P, Xu N, Xie J, Chi J, Feng S, Xu R, Wu M (2001) Mater Res Bull 36:1391
23. Moreira RFPM, Netto GC, Sauer T, José HJ, Humeres E (2004) J Air Waste Manage Assoc 54:77
24. Moreira RFPM, Sauer TP, Casaril L, Humeres E (2005) J Appl Eletrochem 35:821
25. Karkmaz M, Puzenat P, Guillard C, Herrmann JM (2004) Appl Catal B 51:183
26. Gómez V, Larrechi MS, Callao MP (2007) Chemosphere 69:1151
27. Malik PK (2004) J Hazard Mater 113:81
28. Giles CH, D'Silva AP, Easton IAJ (1974) J Colloid Interface Sci 47:766
29. Langmuir I (1918) J Am Chem Soc 40:1361
30. Lou X, Jia X, Xu J, Liu S, Gao Q (2006) Mater Sci Eng A 432:221–225
31. Zhang M, An T, Hu X, Wang C, Sheng G, Fu J (2004) Appl Catal A 260:215